

# Generalized Diffusion Tensor Imaging (GDTI): A Method for Characterizing and Imaging Diffusion Anisotropy Caused by Non-Gaussian Diffusion

CHUNLEI LIU,<sup>a,b</sup> ROLAND BAMMER,<sup>a</sup> AND MICHAEL E. MOSELEY<sup>a,\*</sup>

<sup>a</sup>Richard Lucas MRS/I Center, Department of Radiology, Stanford University, 1201 Welch Road, Stanford, California 94305-5488, USA

<sup>b</sup>Department of Electrical Engineering, 340 Panama Street, Stanford University, Stanford, California 94305-9505, USA

(Received 24 March 2003 and in revised form 6 June 2003)

**Abstract.** For non-Gaussian distributed random displacement, which is common in restricted diffusion, a second-order diffusion tensor is incapable of fully characterizing the diffusion process. The insufficiency of a second-order tensor is evident in the limited capability of diffusion tensor imaging (DTI) in resolving multiple fiber orientations within one voxel of human white matter. A generalized diffusion tensor imaging (GDTI) method was recently proposed to solve this problem by generalizing Fick's law to a higher-order partial differential equation (PDE). The relationship between the higher-order tensor coefficients of the PDE and the higher-order cumulants of the random displacement can be derived. The statistical property of the diffusion process was fully characterized via the higher-order tensor coefficients by reconstructing the probability density function (PDF) of the molecular random displacement. Those higher-order tensor coefficients can be measured using conventional diffusion-weighted imaging or spectroscopy techniques. Simulations demonstrated that this method was capable of quantitatively characterizing non-Gaussian diffusion and accurately resolving multiple fiber orientations. It can be shown that this method is consistent with the  $q$ -space approach. The second-order approximation of GDTI was shown to be DTI.

## INTRODUCTION

In an isotropic medium, the molecular self-diffusion causes the logarithm of the spin echo magnitude to decay linearly as the square of the magnitude of the magnetic field gradient increases.<sup>1</sup> The slope is proportional to the scalar self-diffusion coefficient,  $D$ , and has orientational independence. In contrast, a significant angular dependence of self-diffusion has been observed in various anisotropic media, such as liquid crystals,<sup>2</sup> porous structures,<sup>3</sup> and cat central nervous system.<sup>4</sup> A second-order tensor  $\mathbf{D}$  has been used to characterize this orientational dependence.<sup>5</sup>

The effect of molecular diffusion provides a unique contrast mechanism for magnetic resonance imaging (MRI).<sup>6</sup> Diffusion tensor imaging (DTI) based on the evaluation of the second-order diffusion tensor has become an established imaging modality for studying the microstructure and physiological properties of biological

tissues, especially the brain white matter.<sup>7</sup> The physical basis of DTI is the assumption of the Gaussian distribution of water molecules' random displacement. However, studies have suggested that the molecular random displacement in human brain white matter is no longer Gaussian, and a second-order diffusion tensor is not sufficient to characterize the underlying diffusion process in biological tissues.<sup>8</sup>

In a heterogeneous structure, such as the brain white matter and other porous structures, the translational motion of molecules will be influenced by the confining boundaries. The spatial restriction imposed on the diffusion process means that the probability density function (PDF) of the molecular random displacement may no longer be Gaussian. Consequently, the covariance matrix of the random displacement that depends linearly

\*Author to whom correspondence should be addressed. E-mail: moseley@stanford.edu

on the diffusion tensor is no longer sufficient to characterize the random process, and hence higher-order statistics becomes necessary.

Recently, a generalized diffusion tensor imaging (GDTI) method was proposed for reconstructing the PDF of spin displacement by using its higher-order tensor statistics (HOT), obtainable through conventional diffusion-weighted imaging (DWI) or spectroscopy techniques.<sup>9</sup> In this newly proposed method, a relationship was derived between the complex magnetic resonance signal and the higher-order statistics of the spin displacement. The relationship was then used to reconstruct the PDF of the spin displacement. A second-order approximation of this method has been shown to be equivalent to DTI.

In this article, the capability of the GDTI in characterizing non-Gaussian diffusion is further investigated. The relationship between GDTI and  $\mathbf{q}$ -space imaging is discussed. Some potential experimental difficulties are also pointed out and discussed.

## THEORY

### Generalized Diffusion Equation

The macroscopic theory of Gaussian diffusion is based upon the hypothesis of Fick's first law, which states that the flux of the diffusing substances is proportional to the concentration gradient,<sup>10</sup> i.e.,

$$F_{i_1} = -D_{i_1 i_2} \frac{\partial C}{\partial x_{i_2}}, \quad (i_1, i_2 = 1, 2, 3) \quad (1)$$

where  $F_{i_1}$  is the  $i_1$ -th component of the flux vector,  $C$  is the concentration,  $x_{i_2}$  is the  $i_2$ -th coordinate, and  $D_{i_1 i_2}$  is the element of the second-order self-diffusion tensor. Index notation follows Einstein's summation rule: If an index appears twice in an expression, then summation over that index is implied, as shown in eq 1. The same convention is assumed throughout this manuscript unless the summation is written out explicitly.

As a generalization of Fick's first law, one can write the mathematical relationship as

$$F_{i_1} = -D_{i_1 i_2}^{(2)} \frac{\partial C}{\partial x_{i_2}} - D_{i_1 i_2 i_3}^{(3)} \frac{\partial^2 C}{\partial x_{i_2} \partial x_{i_3}} - D_{i_1 i_2 i_3 i_4}^{(4)} \frac{\partial^3 C}{\partial x_{i_2} \partial x_{i_3} \partial x_{i_4}} - \dots \quad (2)$$

to an arbitrarily high-order partial differentiation of the concentration without opposing the linearity constraint. Here the coefficient  $D_{i_1 i_2 \dots i_n}^{(n)}$  is an  $n$ -th order tensor, where the super-index  $n$  in the parenthesis indicates the order of the tensor, and the sub-index indicates the coordinate.

Those coefficients relate the flux to the  $n$ -th order partial differentiation of the particle concentration. Higher-order coefficients become necessary when the diffusion is non-Gaussian, which will be shown. For Gaussian diffusion processes, the higher-order coefficients are zero, i.e.,

$$D_{i_1 i_2 \dots i_n}^{(n)} = 0, \quad (\text{for } n \geq 3)$$

Under this condition, eq 2 reduces to the usual form of Fick's first law. By using the following standard mathematical notation,

$$\nabla_{i_1 i_2 \dots i_n} = \frac{\partial^n}{\partial x_{i_1} \partial x_{i_2} \dots \partial x_{i_n}}$$

eq 2 can be written as

$$F_{i_1} = -D_{i_1 i_2}^{(2)} \nabla_{i_2} C - D_{i_1 i_2 i_3}^{(3)} \nabla_{i_2 i_3} C - D_{i_1 i_2 i_3 i_4}^{(4)} \nabla_{i_2 i_3 i_4} C - \dots \quad (3)$$

After applying the continuity theorem, one obtains the following generalized partial differential equation for diffusion:

$$\frac{\partial C}{\partial t} = -\nabla_{i_1} F_{i_1} = D_{i_1 i_2}^{(2)} \nabla_{i_1 i_2} C + D_{i_1 i_2 i_3}^{(3)} \nabla_{i_1 i_2 i_3} C + D_{i_1 i_2 i_3 i_4}^{(4)} \nabla_{i_1 i_2 i_3 i_4} C + \dots \quad (4)$$

which is basically a generalization of Fick's second law. In obtaining the last equality,  $D_{i_1 i_2 \dots i_n}^{(n)}$  tensors are assumed to be spatially invariant for a given voxel of interest. Equation 4 can be derived formally assuming a Markov property of the diffusion process by generalizing the Kramers–Moyal expansion to a multivariate case.<sup>11,16</sup>

The macroscopic nuclear magnetization density vector  $\mathbf{M}(\mathbf{x}, t)$  is proportional to the spin concentration, so considering the spin diffusion, one can write the Bloch equation in the rotating frame as

$$\frac{\partial \mathbf{M}(\mathbf{x}, t)}{\partial t} = \gamma \mathbf{M}(\mathbf{x}, t) \times \mathbf{B}(\mathbf{x}, t) - \frac{M_1 \mathbf{e}_1 + M_2 \mathbf{e}_2}{T_2} - \frac{M_3 - M(0)}{T_1} \mathbf{e}_3 + D_{i_1 i_2}^{(2)} \nabla_{i_1 i_2} \mathbf{M} + D_{i_1 i_2 i_3}^{(3)} \nabla_{i_1 i_2 i_3} \mathbf{M} + D_{i_1 i_2 i_3 i_4}^{(4)} \nabla_{i_1 i_2 i_3 i_4} \mathbf{M} + \dots \quad (5)$$

Here,  $\mathbf{B}(\mathbf{x}, t)$  is the applied magnetic field strength,  $\mathbf{e}_i$ 's are a set of orthogonal unit vectors that spans the 3D real space, and  $M_i$  ( $i = 1, 2, 3$ ) is the component of

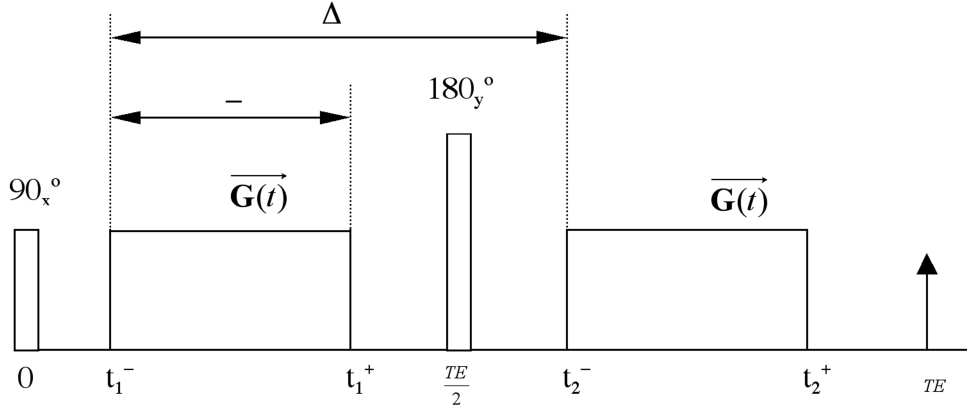


Fig. 1. Time diagram for a spin echo sequence with diffusion encoding gradients.

$\mathbf{M}(\mathbf{x}, t)$  along  $\mathbf{e}_i$ . For the sequence depicted in Fig. 1, by solving the above equation the transverse magnetization was found to be<sup>9</sup>

$$m(b) = m(0) \exp\left(\sum_{n=2}^{\infty} (+j)^n D_{i_1 i_2 \dots i_n}^{(n)} b_{i_1 i_2 \dots i_n}^{(n)}\right) \quad (6)$$

where  $m(0)$  is the transverse magnetization measured at TE (echo time) in the absence of diffusion gradient, and  $j$  is the square root of  $-1$ . The elements of tensor  $b^{(n)}$  are defined as<sup>9</sup>

$$b_{i_1 i_2 \dots i_n}^{(n)} = \int_{t_1^-}^{t_2^-} k_{i_1}(\tau) k_{i_2}(\tau) \dots k_{i_n}(\tau) d\tau + (-1)^n \times \int_{t_2^+}^{TE} \kappa_{i_1}(\tau) \kappa_{i_2}(\tau) \dots \kappa_{i_n}(\tau) d\tau \quad (7)$$

where  $\mathbf{k}(t)$  and  $\kappa(t)$  are defined as

$$\mathbf{k}(t) = \gamma \int_0^t \mathbf{G}(\tau) d\tau \quad (8)$$

$$\kappa(t) = \mathbf{k}(t) - 2\mathbf{k}(t_1^+) \quad (9)$$

Here,  $t_1^-$  and  $t_1^+$  are the starting and ending times, respectively, for the first diffusion gradient lobe.  $t_2^-$  and  $t_2^+$  are defined similarly, as shown in Fig. 1.

If the diffusion gradients are constant over time, it can be shown that<sup>9</sup>

$$b_{i_1 i_2 \dots i_n}^{(n)} = \gamma^n G_{i_1} G_{i_2} \dots G_{i_n} \delta^n \left( \Delta - \frac{n-1}{n+1} \delta \right) \quad (10)$$

Notice that for  $n = 2$ , eq 10 becomes the familiar  $b$  matrix.<sup>7</sup>

$$b_{i_1 i_2} = \gamma^2 G_{i_1} G_{i_2} \delta^2 \left( \Delta - \frac{1}{3} \delta \right) \quad (11)$$

Equation 6 shows that even-order tensors only affect the magnitude of the signal whereas odd-order tensors only affect the phase of the signal.

#### The Relationship Between $D^{(n)}$ Tensors and Higher-Order Statistics

Consider a spin echo sequence with narrow diffusion gradient pulses, i.e., the  $\mathbf{q}$ -space approach.<sup>3</sup> Define  $\mathbf{q} = \gamma \delta \mathbf{G}$ , then the signal intensity as a function of  $\mathbf{q}$  can be written as<sup>3</sup>

$$m(\mathbf{q}) = m(0) \int P(\mathbf{r}, \Delta) \exp(-j \mathbf{q} \cdot \mathbf{r}) d\mathbf{r} \quad (12)$$

where  $P(\mathbf{r}, \Delta)$  is the PDF of the spin displacement  $\mathbf{r}$  during the gradient separation time interval  $\Delta$ . Hence,  $m(\mathbf{q})/m(0)$  is the characteristic function of the random displacement vector  $\mathbf{r}$ , i.e., the Fourier transformation of the PDF. In general, the characteristic function can be expanded as an exponential function of a series of cumulants as<sup>12</sup>

$$\frac{m(\mathbf{q})}{m(0)} = \exp\left(\frac{(-j) Q_{i_1}^{(1)} q_{i_1}}{1!} + \frac{(-j)^2 Q_{i_1 i_2}^{(2)} q_{i_1} q_{i_2}}{2!} + \dots + \frac{(-j)^n Q_{i_1 i_2 \dots i_n}^{(n)} q_{i_1} q_{i_2} \dots q_{i_n}}{n!} + \dots\right) \quad (13)$$

where  $q_i$  is the  $i$ -th component of the vector  $\mathbf{q}$ . The expansion coefficient  $Q_{i_1 i_2 \dots i_n}^{(n)}$  is defined as the  $n$ -th order cumulant of the random variable  $\mathbf{r}(\Delta)$ . By comparing eq 13 to eq 6,  $Q_{i_1 i_2 \dots i_n}^{(n)}$  was found to be proportional to  $D_{i_1 i_2 \dots i_n}^{(n)}$ <sup>9</sup>

$$Q_{i_1 i_2 \dots i_n}^{(n)} = (-1)^n n! D_{i_1 i_2 \dots i_n}^{(n)} \left( \Delta - \frac{n-1}{n+1} \delta \right) \approx (-1)^n n! D_{i_1 i_2 \dots i_n}^{(n)} \Delta \quad (14)$$

where  $\Delta$  is the separation time of the two diffusion gradients, and  $\delta$  is the duration of each gradient lobe.

For the case that  $\mathbf{r}$  is a zero mean Gaussian random variable, all but the second-order cumulants are zero.<sup>12</sup> This result can be easily obtained based on the observation that the Fourier transformation of a Gaussian function remains Gaussian.<sup>13</sup> Under this condition, eq 6 reduces to the familiar ordinary signal equation in DTI,

$$\frac{m(TE)}{m(0)} = \exp\left(-b_{i_1 i_2} D_{i_1 i_2}\right) \quad (15)$$

### PDF Reconstruction

Two methods are commonly used to obtain the probability density function of a random variable via its higher-order statistics: Edgeworth series expansion and Gram–Charlier series expansion.<sup>12</sup> Edgeworth series does not have a closed form Fourier transformation, but Gram–Charlier series does.<sup>12</sup> In fact, Gram–Charlier series is the Fourier expansion of the PDF. As mentioned in the previous section, the MR signal measured is the Fourier transformation of the PDF. Hence, it is more convenient to use the Gram–Charlier series to represent the PDF in this context. Using higher-order cumulants, the PDF of the spin displacement  $\mathbf{r}$  can be reconstructed via the Gram–Charlier series<sup>12,14</sup> as follows:

$$P(\mathbf{r}) = N\left(0, Q_{i_1 i_2}^{(2)}\right) \times \left(1 + \frac{Q_{i_1 i_2 i_3}^{(3)}}{3!} H_{i_1 i_2 i_3}(\mathbf{r}) + \frac{Q_{i_1 i_2 i_3 i_4}^{(4)}}{4!} H_{i_1 i_2 i_3 i_4}(\mathbf{r}) + \dots\right) \quad (16)$$

where  $N(0, Q_{i_1 i_2}^{(2)})$  is the normal distribution with zero mean and covariance matrix  $Q_{i_1 i_2}^{(2)}$ , and  $H_{i_1 i_2 \dots i_n}(\mathbf{r})$  is the  $n$ -th order Hermite tensor.<sup>12,14</sup> The third and fourth Hermite tensor are reproduced here as a matter of completeness. Let  $P_{i_1 i_2}$  be the component of  $N(0, Q_{i_1 i_2}^{(2)})^{-1}$ , i.e., the inverse of the covariance matrix. If we set  $w_{i_1} \equiv P_{i_1 i_2} r_{i_2}$ , then the components of the third and fourth Hermite tensor may be written<sup>15</sup>

$$\begin{aligned} H_{i_1 i_2 i_3}(\mathbf{r}) &= w_{i_1} w_{i_2} w_{i_3} - (w_{i_1} P_{i_2 i_3} + w_{i_2} P_{i_1 i_3} + w_{i_3} P_{i_1 i_2}) \\ &= w_{i_1} w_{i_2} w_{i_3} - 3 w_{(i_1} P_{i_2 i_3)} \end{aligned} \quad (17)$$

$$\begin{aligned} H_{i_1 i_2 i_3 i_4}(\mathbf{r}) &= w_{i_1} w_{i_2} w_{i_3} w_{i_4} - 6 w_{(i_1} w_{i_2} P_{i_3 i_4)} \\ &+ 3 P_{(i_1 i_2} P_{i_3 i_4)} \end{aligned} \quad (18)$$

where indices in parentheses designate that the term is to be averaged over all permutations of those indices that produce different terms, remembering that  $P_{i_1 i_2} = P_{i_2 i_1}$  and  $w_{i_1} w_{i_2} = w_{i_2} w_{i_1}$ , as illustrated for  $H_{i_1 i_2 i_3}(\mathbf{r})$  in eq 17.

For example,  $w_{i_1} w_{i_2} P_{i_3 i_4} = w_{i_1} w_{i_2} P_{i_4 i_3}$ , hence this permutation does not produce a different term. Although cumulants  $Q_{i_1 i_2 \dots i_n}^{(n)}$  are not directly MR-measurable quantities, they can be indirectly determined from MR-measurable quantities  $D_{i_1 i_2 \dots i_n}^{(n)}$  via eq 14. The shape of the reconstructed PDF can then be used to infer the microstructure of the media.

A well-documented problem of this approach is that the reconstructed PDF is not always non-negative.<sup>16,17</sup> There are two issues related to this problem. First, in practice, for the purpose of tractability, the infinite series in eq 4 has to be truncated to a finite order. This truncation assumes that terms above a given order are zero. However, Pawula has shown that this assumption implies that all terms above second order are zero.<sup>16</sup> If one ignores the difficulties of the mathematical justification of the truncation process, the truncated version of eq 4 can be solved given the boundary condition and the solution can be used to approximate the true PDF. However, the approximation may not always be non-negative.<sup>16</sup> Second, the Gram–Charlier series of finite number of terms may not always be non-negative at certain areas, even if the higher-order cumulants are of their true values.<sup>17</sup> The negative region usually appears at places far away from the mean position of the random displacement. The result usually is tolerable, as demonstrated later by computer simulations, since one usually is only interested in the region close to the mean value of the displacement. Nevertheless, one has to consider the possible error in the reconstructed PDF when interpolating the experimental result.

Despite the difficulty discussed above, the method of using higher-order statistics to reconstruct a non-Gaussian PDF has been a common practice in various fields of physical sciences. For example, Johnson has introduced the higher cumulants to interpret X-ray diffraction data in crystallography.<sup>17a</sup> He found that the non-Gaussian motion in crystals can be characterized by the higher-order cumulants.<sup>17</sup> Applications can also be found in the field of astronomy and astrophysics, where higher-order statistics is used for studying cosmic microwave background anisotropies,<sup>18</sup> and for analyzing the velocity distributions and fine structure in elliptical galaxies.<sup>18</sup>

## EXPERIMENTAL

### Computer Simulation

A series of MR experiments was simulated on four synthetic phantoms that have simple structures. The four phantoms are (Fig. 2): (a) an isotropic phantom, (b) a single tube, (c) an X-shaped tube, and (d) a Y-shaped tube. All the tubes have square cross sections with a width of 40  $\mu\text{m}$ , which is roughly on the order of the diameter of larger-sized human nerve fibers.<sup>19</sup> The boundaries of the tubes were assumed to be impermeable.

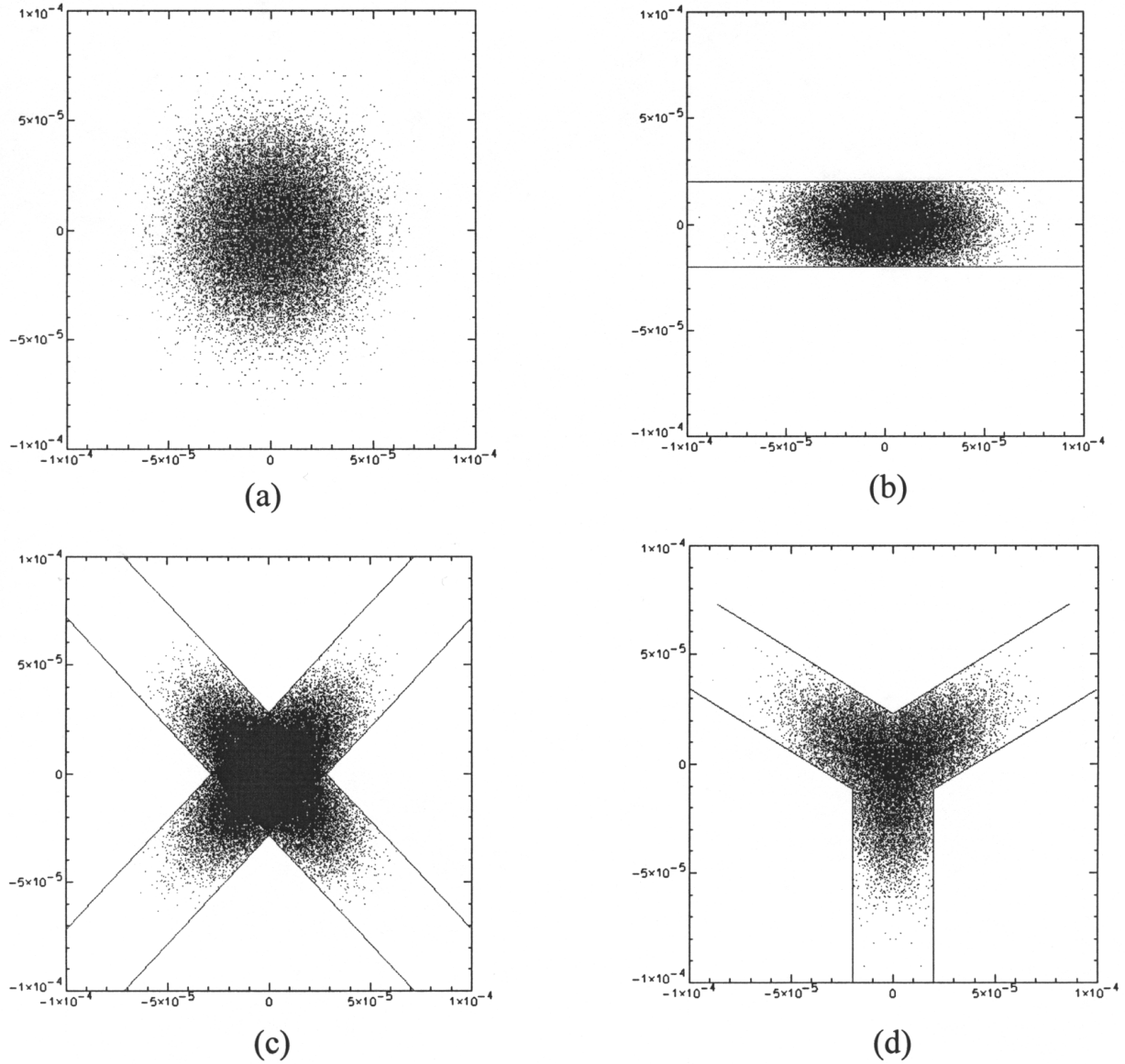


Fig. 2. A cross-sectional view in the XY plane of four 3D synthetic phantoms. The dots are simulated random spin displacements with initial position at the origin. (a) Phantom 1, isotropic; (b) Phantom 2, single tube; (c) Phantom 3, X-shaped tube; (d) Phantom 4, Y-shaped tube. In Phantom 1, spins are allowed to diffuse freely. Phantoms 2–4 are confined by the boundaries drawn as solid lines.

Imaging sequence parameters were chosen to be comparable to those used in real *in vivo* experiments, and were kept the same throughout all the simulations. The duration  $\delta = 20.2$  ms and the separation time  $\Delta = 100.5$  ms. The separation time is slightly larger than what was normally used in most sequences,<sup>20</sup> in order to assure that  $\Delta$  was much larger than  $\delta$  and to increase the likelihood that spins experience motional restriction due to the confining vessel walls. This yielded an effective diffusion time of 93.8 ms. The maximum diffusion gradient strength used was 40 mT/m, which was roughly the

maximum value currently offered by most whole body systems. For free diffusion, the diffusion coefficient  $D$  was set to be  $2.02 \times 10^{-3}$  mm<sup>2</sup>/s, which is comparable to the free self-diffusion coefficient of water at about 20 °C.

For each phantom, a corresponding distribution of the spin displacement  $\mathbf{r}_i$  was generated by using an algorithm similar to that of Balinov et al.<sup>21</sup> Assuming a spin echo sequence, the accumulated phase and corresponding signal can be computed as follows:<sup>3,21</sup>

$$\Phi_i = \gamma \delta \mathbf{G} \cdot \mathbf{r}_i \quad (19)$$

$$S = \frac{1}{N} \sum_{i=1}^N e^{-j\Phi_i} \quad (20)$$

where  $\mathbf{G}$  is the diffusion gradient vector and is assumed constant,  $\mathbf{r}_i$  is the generated  $i$ -th spin displacement,  $\Phi_i$  is the corresponding accumulated phase due to diffusion,  $N$  is the total number of generated spin displacements ( $N = 240,000$  in this simulation), and  $S$  is the complex signal. Notice that the signal attenuation due to  $T_1$  and  $T_2$  decay has been neglected.

Since the complex signal  $S$  is not only a function of the magnitude of the diffusion gradient but also a function of its direction, with the gradient timing fixed, a sound estimation of the tensor elements will therefore require variations of both the magnitude and direction of the gradients over a sufficiently wide range. In this simulation, 200 gradient directions were used and they were evenly distributed on the surface of a sphere. At each orientation, the gradient strength was varied from 0–40 mT/m in 10 uniform steps.

#### Data Analysis

The  $D_{i_1 i_2 \dots i_n}^{(n)}$  tensors were estimated by combining a series of experiments with different diffusion gradient vectors and solving the following set of linear equations derived from eq 6 (see eq 21 at bottom of page).

Note that  $S/S_0$  is a complex number in general. In principle, the  $D_{i_1 i_2 \dots i_n}^{(n)}$  tensors can then be determined to an arbitrarily high order by truncating the series summation to the desired order number.

The symmetry property of the  $D_{i_1 i_2 \dots i_n}^{(n)}$  tensors could greatly reduce the complexity of the estimation problem. By definition,  $b_{i_1 i_2 \dots i_n}^{(n)}$  is a symmetric tensor, which means that the order of the subscripts will not affect the values of the tensor elements. From eq 21 it is evident that  $D_{i_1 i_2 \dots i_n}^{(n)}$  is also a symmetric tensor. In general, a symmetric tensor in 3D real space of order  $n$  has  $(n+1)(n+2)/2$  independent elements out of the total  $3^n$  elements.<sup>14</sup> Hence, due to the symmetry, the number of tensor elements that needs to be estimated is greatly reduced. For example, to determine a tensor of order 4, only its 15 independent elements instead of its total number of elements, 81, need to be estimated. Although the symmetry constraint reduces the number of independent elements for each tensor, the total number of independent tensor elements (the total free parameters) that needs to be estimated grows fairly rapidly with the order of the approximation. Table 1 lists the total number of independent tensor elements that needs to be estimated for order 1 to 6 approximations of the cumulant expansion.

For the simulation, a total of 2000 (200 gradient directions  $\times$  10 gradient strengths) linear equations were obtained. The

$$\ln\left(\frac{S}{S_0}\right) = -b_{i_1 i_2}^{(2)} D_{i_1 i_2}^{(2)} + b_{i_1 i_2 i_3 i_4}^{(4)} D_{i_1 i_2 i_3 i_4}^{(4)} - \dots + (-1)^n b_{i_1 i_2 \dots i_{2n}}^{(2n)} D_{i_1 i_2 \dots i_{2n}}^{(2n)} + \dots \\ + j \left( -b_{i_1 i_2 i_3}^{(3)} D_{i_1 i_2 i_3}^{(3)} + b_{i_1 i_2 i_3 i_4 i_5}^{(5)} D_{i_1 i_2 i_3 i_4 i_5}^{(5)} - \dots + (-1)^n b_{i_1 i_2 \dots i_{2n+1}}^{(2n+1)} D_{i_1 i_2 \dots i_{2n+1}}^{(2n+1)} + \dots \right) \quad (21)$$

Table 1. Total number of independent tensor elements to estimate for each order approximation of the cumulant expansion\*

order of the cumulant expansion	total number of independent tensor elements
1	1
2	6
3	16
4	31
5	52
6	80

\*The first-order approximation corresponds to an isotropic Gaussian diffusion model; in this approximation only the diffusion coefficient  $D$  needs to estimate. The second-order approximation corresponds to the DTI Gaussian model, where a second-order tensor needs to be estimated. In the third-order approximation, where non-Gaussian diffusion is assumed, both the second-order (with 6 independent elements) and the third-order tensors (with 10 independent elements) need to be estimated with a total number of independent elements of 16, and so on.

$D_{i_1 i_2 \dots i_n}^{(n)}$  tensors up to order 4 were estimated using the singular value decomposition (SVD) method<sup>22</sup> by rewriting the series of linear equations in a matrix format.

#### Visualization

Using the estimated  $D_{i_1 i_2 \dots i_n}^{(n)}$  tensors, the PDF of spin displacement was reconstructed via eq 16. For visualization purposes, two rendering techniques were used: (i) iso-surface plot of the PDF, and (ii) iso-surface plot of the deviation of the PDF from Gaussian PDF. The latter is called the skewness and kurtosis map (skewness map for simplicity), which is determined via the following equation:

$$\Delta P(r) = P(\mathbf{r}) - N(0, Q_{i_1 i_2}^{(2)}) = \\ N(0, Q_{i_1 i_2}^{(2)}) \left( \frac{Q_{i_1 i_2 i_3}^{(3)}}{3!} H_{i_1 i_2 i_3}(\mathbf{r}) + \frac{Q_{i_1 i_2 i_3 i_4}^{(4)}}{4!} H_{i_1 i_2 i_3 i_4}(\mathbf{r}) + \dots \right) \quad (22)$$

For easy recognition of the positive and negative values, grayscale-coding is introduced in the skewness map where silver represents positive values and dark represents negative values.

## RESULTS AND DISCUSSION

### Simulation Result

The resultant PDF iso-surface plots and the skewness maps obtained from the four phantoms were plotted in Fig. 3. The diffusion ellipsoid determined by DTI was also shown in this figure as a side-by-side comparison. The skewness map is plotted in two ways: in the first plot, the negative part (dark) is made transparent while the positive part (silver) is solid; in the other plot, both parts are made solid. All the plots are 3D objects.

For the isotropic phantom 1, both methods produced an almost identical result, which confirmed the orientational independence of isotropic diffusion. Phantom 2 contained a single rectangular tube. This feature was fully conveyed in both the skewness map and PDF iso-

surface plot. The accuracy of the GDTI method was well demonstrated by the square cross-section of the skewness map. While DTI was capable of revealing the fact that spin diffused faster along the tube, some subtleties were lost because only the magnitude of the signal can be utilized. Phantoms 3 and 4 had more complex structures. Both had several diffusion branches, while phantom 3 was symmetric and phantom 4 was asymmetric. Nevertheless, both the skewness map and PDF iso-surface plot were able to determine the shape of the phantoms. Although the rectangular shape of the tube and the symmetry of the structure were not reproduced perfectly, the plots have been sufficient to represent the overall geometrical structure of the phantom. The imperfection was caused by the intrinsic randomness of the diffusion process, the insufficient diffusion exposure

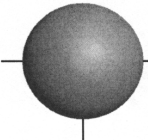
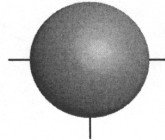
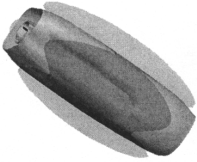
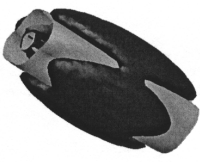
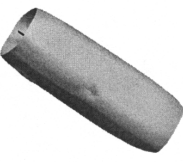
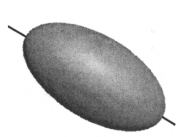
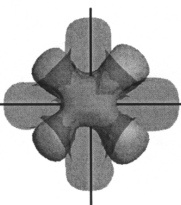
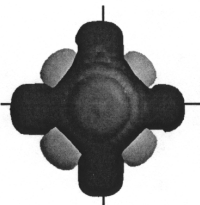
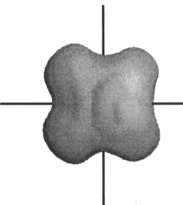
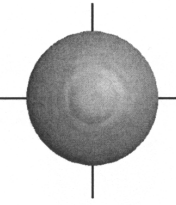
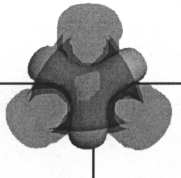
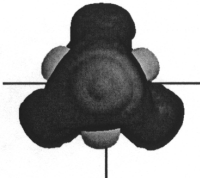
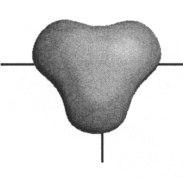
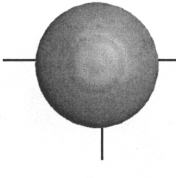
Phantom #	GDTI		DTI
	PDF skewness map	PDF iso-surface	Diffusion ellipsoid
1 Isotropic			
2 Single tube	 		
3 X-shaped tube	 		
4 Y-shaped tube	 		

Fig. 3. Phantom simulation results. For the isotropic phantom, the skewness is negligible and not plotted here. In the PDF and diffusion ellipsoid plots, the lines are x and y-axis. In the PDF skewness map, silver indicates positive skewness and dark represents negative skewness. Note that the dark area is plotted transparent in the first column of the skewness maps and solid in the second column. The PDF skewness maps and the PDF iso-surface plots are similar to the geometric shape of the respective phantom. The diffusion ellipsoid fails to reveal the structure of phantom 3 and 4.

time, and the increasing complexity of the structure. On the other hand, the diffusion ellipsoid, which only utilized the second-order diffusion tensor, was unable to correctly represent the diffusion anisotropy possessed by the spin inside the tube.

#### Relationship Between GDTI and DTI

DTI uses a second-order diffusion tensor to characterize the diffusion anisotropy by assuming Gaussian diffusion. DTI has been successfully applied in clinical settings and has become an important imaging modality. The limitations of the DTI model, however, have been generally neglected or were not widely known. When the diffusion is of non-Gaussian type, a second-order diffusion tensor is not the correct model to fit the experimental data. Thus, the information obtained could be inaccurate or even misleading, as demonstrated by the simulation. More specifically, the second-order diffusion tensor is symmetric; hence, it cannot fully represent asymmetric structures. The second-order tensor has only one orientational maximum, i.e., the major eigenvalue; hence, it cannot resolve multiple diffusion orientations. In the presence of non-Gaussian diffusion, the measured diffusion tensor will depend on the set of direction of the diffusion gradients applied; hence, it varies with diffusion gradient directions used. These facts will set the limitations for the DTI method.

The GDTI, as an extension to DTI, does not assume any particular diffusion model. It utilizes the higher-order statistics to characterize the random diffusion process. Physically it is consistent with the  $\mathbf{q}$ -space approach, as shown in the theory section. The PDF obtained by using GDTI method is an approximation to the true probability function, since in practice one has to truncate the summation series in order to compute the higher-order tensors. In principle, however, one could make the approximation as accurate as desired by going to higher-order tensors. Usually, tensors up to order 4 would make a good approximation.

The importance of using higher-order tensors to probe the microstructure can be appreciated most from the simulation results of phantom 4. In this case, the PDF of the random spin displacement is not an even function. Generally, every function can be written as the combination of its even part and odd part.<sup>13</sup> The even part has a real and even Fourier transformation, whereas the odd part has an imaginary and odd Fourier transformation.<sup>13</sup> Hence, the signal is generally complex. As shown in the theory section, DTI is a second-order approximation of the GDTI method. In other words, it utilizes only the quadratic part of the MR signal. The inadequacy of this approximation is well seen in phantoms 3 and 4.

#### Relationship Between GDTI and $\mathbf{q}$ -space Imaging

The  $\mathbf{q}$ -space imaging method does not assume a particular diffusion model and hence is principally accurate in probing the complex microstructures. It has been shown that the GDTI is consistent with  $\mathbf{q}$ -space imaging; however, the measurement of the higher-order diffusion tensors, i.e., the  $D_{i_1 i_2 \dots i_n}^{(n)}$  tensors, does not require that the strict assumption of  $\mathbf{q}$ -space imaging be satisfied. Only the estimation of the higher-order cumulants, i.e., the  $Q_{i_1 i_2 \dots i_n}^{(n)}$  tensors, relies on the justification of  $\mathbf{q}$ -space imaging. Although there is concern regarding the feasibility of  $\mathbf{q}$ -space imaging,<sup>23</sup> a few early studies have reported that the  $\mathbf{q}$ -space imaging can be performed practically.<sup>24</sup> Anyhow, the accuracy of the reconstructed PDF by GDTI will depend on how well the relationship between  $Q_{i_1 i_2 \dots i_n}^{(n)}$  and  $D_{i_1 i_2 \dots i_n}^{(n)}$  holds. Nevertheless, the measurement of the higher-order tensorial coefficients  $D_{i_1 i_2 \dots i_n}^{(n)}$  alone provides a unique method to quantitatively characterize the non-Gaussianity of a diffusion process. Being able to quantitatively characterize the non-Gaussianity is one advantage of the GDTI method.

Many numerical quantities can be derived from the higher-order tensors. For example, the full information content of the higher-order tensors can be condensed to provide single numbers for a discussion of the properties of the underlying diffusion process. A very useful operation in this respect is tensor contraction.<sup>25</sup> Full contraction of an even-order tensor of rank  $n$  is defined as

$$I^{(n)} = g_{i_1 i_2} g_{i_3 i_4} \dots g_{i_{n-1} i_n} D_{i_1 i_2 \dots i_n}^{(n)} \quad (23)$$

where  $g_{kl}$  is the real-space metric tensor. For a Cartesian coordinate,  $g_{kl}$  is an identity matrix. The scalar invariant  $I^{(n)}$  is also called the trace of a tensor of rank  $n$ . For even-order tensors of rank above 2, negative trace-values indicate flatness of the PDF, while positive values indicate peakedness of the PDF compared with a Gaussian distribution with the same covariance matrix.

Because of the finite voxel size, the PDF imaged by GDTI and  $\mathbf{q}$ -space imaging is the PDF of the random displacement averaged over all starting positions.<sup>3</sup> In the long time limit, i.e.,  $\Delta \rightarrow \infty$ , the PDF of the spin random displacement is the autocorrelation function of the spin density.<sup>3</sup> Consequently, the measured MR signal, as the Fourier transformation of the PDF (see eq 12), is an even and real function. As a result, the odd-order tensors are null in the long time limit, hence some information of the underlying microstructures is lost. This is an intrinsic disadvantage of the MR diffusion experiment, whether one uses GDTI or  $\mathbf{q}$ -space imaging.<sup>3</sup>

#### Some Practical Issues

In order to measure the higher-order tensors of both even and odd rank, one has to collect the full complex



MR signals instead of only the magnitude. Although even-order tensors only affect the magnitude, and odd-order tensors are only present in the phase of the signal, the accuracy of the estimation for both types of tensors is the same because of the particular estimation method we used. In this estimation method, the full complex signal is utilized instead of separating the magnitude signal from the phase signal. By doing this, magnitude and phase information are both present in the real and imaginary parts of the signal, and the error of estimation is therefore spread. Consequently, phase wrapping is also not a problem, since the phase only appears in the trigonometric functions.

An accurate estimation of the odd-order tensors requires correct phase information of the signal. There are various sources that could introduce phase error in an in vivo experiment, such as eddy current and subject movement. Eliminating or correcting those phase errors is still a difficult task. To reduce the estimation error, one should use more b-values. As seen in eq 21, the signal is a smooth function of the b tensors, and phase error introduced by subject movement is random. With more b-values used, the random errors can be averaged out. Thus, the effect of phase error can be reduced. Nevertheless, great care has to be exercised when interpreting the odd-order tensors when phase error is significant.

Noise is always present in any MR measurement. This noise is usually modeled as Gaussian distributed and additive. The effect of this additive noise on the estimation of higher-order tensors can be analyzed analytically through eq 6. In general, the presence of noise will degrade the accuracy of the estimated higher-order tensors and hence cause distortion in the PDF skewness map. A certain level of SNR (ratio of signal amplitude to noise standard deviation) has to be maintained in order to obtain a reasonably accurate skewness map. Simulations show that when SNR is higher than 7, all the phantom structures used in this study can be reconstructed reasonably well.

Another aspect of designing a GDTI measurement is the choice of b-values. When the diffusion time is short, most spins do not experience the restriction imposed by the boundaries. In this case, the measured displacement distribution approaches a Gaussian function. Therefore, in order to measure the higher-order tensors, one has to ensure that the diffusion time is long enough so that most spins would experience the boundary effect. A rough guideline is that the resultant mean displacement of the spin is on the order of the size of the capillary. Because of the three-dimensional nature of the PDF, the diffusion gradients have to be applied in a set of uniformly sampled 3D directions in the absence of a priori information of the PDF. Unfortunately, this will necessarily lengthen the data collection time. Our initial pro-

cedure for in vivo human brain study utilizes 58 gradient directions and 4 b-values (maximum  $b = 4000 \text{ s/mm}^2$ ) for each direction. With  $TR = 4\text{s}$ , the total scan time is approximately 15 minutes.

### Potential Applications

Because of its ability to characterize non-Gaussian diffusion, GDTI can potentially provide a useful technique for probing microstructures where restricted diffusion is common. One application would be probing the structures of porous media (nanotube bundles, foam, lung, oil- and natural-gas-bearing reservoir rocks, etc.).<sup>3</sup> By reconstructing the probability distribution function of the liquid or gas molecular random displacement, information can be extracted not only about the molecular motion, but also about the geometry of the boundaries and, hence, about the pore morphology of the surrounding media.

A second application for GDTI is neuroimaging. The water diffusion in the white matter is non-Gaussian because of the restriction imposed by fiber boundaries, as suggested by earlier reports.<sup>8</sup> By imaging higher-order tensors, one can obtain not only a more accurate description of the underlying diffusion process, but also better knowledge of the fiber connectivity information. As a result, GDTI could considerably improve the ability of MRI to detect the intersecting fibers and, thus, could potentially improve fiber tractography.<sup>26</sup>

### CONCLUSIONS

In summary, a Gaussian random variable is completely characterized by its covariance matrix; hence, a second-order diffusion tensor is sufficient to represent a Gaussian diffusion process. However, higher-order statistics are required in order to fully characterize a non-Gaussian random variable, hence higher-order diffusion tensors are necessary for the characterization of the diffusion anisotropy caused by a non-Gaussian diffusion process. By relating the MR measurable higher-order diffusion tensors and the higher-order statistics, GDTI provides a means for quantitatively characterizing non-Gaussian diffusion. Thus, GDTI could potentially be a useful technique for studying complex physical and biological microstructures.

*Acknowledgments.* This work was supported in part by the National Institute of Health NIH-1R01NS35959, the center of Advanced MR Technology of Stanford (NCRR P41 RR 09784), and the Lucas Foundation. The authors thank the anonymous reviewer for pointing out a reference to Kramers–Moyal expansion and Karen Chen for proofreading the manuscript.

### REFERENCES AND NOTES

- (1) Hahn, E.L. *Phys. Rev.* **1950**, *80*, 580.
- (2) Blinc, R.; Burgar, M.; Luzar, M.; Pirs, J.; Zupancic, I.;

- Zumer, S. *Phys. Rev. Lett.* **1974**, *33*, 1192.
- (3) Callaghan P.T. *Principles of Nuclear Magnetic Resonance Microscopy*; Oxford Science Publication: New York, 1991, Chapter 7.
- (4) (a) Moseley, M.E.; Cohen, Y.; Kucharczyk, J. *Radiology* **1990**, *176*, 439–446. (b) Moseley, M.E.; Cohen, Y.; Kucharczyk, J. *Magn. Reson. Med.* **1990**, *14*, 330–346.
- (5) (a) Stejskal, E.O.; Tanner, J.E. *J. Chem. Phys.* **1965**, *42*, 288. (b) Turner, R.; LeBihan, D.; Maier, J.; Vavrek, R.; Hedges, L.K.; Pekar, J. *Radiology* **1990**, *177*, 407. (c) Basser, P.J.; Mattiello, J.; Turner, R.; Le Bihan, D. In *Proceedings of the SMRM*; 1993, p 584.
- (6) (a) Merboldt, K.D.; Hanicke, W.; Frahm, J. *J. Magn. Reson.* **1985**, *64*, 479–486. (b) Le Bihan, D.; Breton, E.; Lallemand, D.; Grenier, P.; Cabanis, E.; Laval-Jeantet, M. *Radiology* **1986**, *161*, 401–407.
- (7) Basser, P.J.; Mattiello, J.; Le Bihan, D. *Biophys. J.* **1994**, *66*, 259–267.
- (8) (a) Tuch, D.S.; Weisskoff, R.M.; Belliveau, J.W.; Wedeen, V.J. In *Proceedings 7th Annual Meeting of ISMRM*; Philadelphia, 1999. p 321. (b) Tuch, D.S.; Reese, T.G.; Wiegell, M.R.; Makris, N.; Belliveau, J.W.; Wedeen, V.J. *Magn. Reson. Med.* **2002**, *48*, 577–582.
- (9) (a) Liu, C.; Bammer, R.; Acar, B.; Moseley, M.E. In *Proceedings 11th Annual Meeting of ISMRM*; Toronto, 2003. (b) Liu, C.; Bammer, R.; Acar, B.; Moseley, M.E. Generalized Diffusion Tensor Imaging (GDTI): Using Higher Order Tensor (HOT) Statistics. Submitted for publication.
- (10) Fick, A. *Ann. Phys.* **1855**, *170*, 59.
- (11) (a) Kramers, H.A. *Physica* **1940**, *7*, 284. (b) Moyal, J.E. *J. R. Stat. Soc. London* **1949**, *B11*, 150.
- (12) Kendall, M.B.; Stuart, A. *The Advanced Theory of Statistics*; Halsted Press: New York, 1994; Vol. 1.
- (13) Bracewell, R. *The Fourier Transform and Its Application*, 3rd ed.; McGraw-Hill Higher Education: Boston, 2000.
- (14) McCullagh, P. *Tensor Methods in Statistics*; Chapman & Hall: New York, 1987.
- (15) Kuznetsov, P.I.; Stratonovich, R.L.; Tikhonov, V.I. *Theory Probab. Appl.* 1960, *5*, 80 (English Translation Series).
- (16) Pawula, R.F. *Phys. Rev.* **1967**, *162*, 186–188.
- (17) (a) Johnson, C.K. *Acta Cryst.* **1969**, *A25*, 187–194. (b) Zucker, U.H.; Schulz, H. *Acta Cryst.* **1982**, *A38*, 563–568. (c) Zucker, U.H.; Schulz, H. *Acta Cryst.* **1982**, *A38*: 568–576.
- (18) (a) Scherrer, R.; Bertschinger, E. *Astrophys. J.* **1992**, *381*, 349. (b) Heyl, J.S.; Hernquist, L.; Spergel, D.N. *Astrophys. J.* **1994**, *427*, 165.
- (19) Kandel, E.R.; Schwartz, J.H. *Principles of Neural Science*, 2nd ed.; Elsevier: New York, 1985.
- (20) Mattiello, J.; Basser, P.J.; Le Bihan, D. *Magn. Reson. Med.* **1997**, *37*, 292–300.
- (21) Balinov, B.; Jönsson, B.; Linse, P.; Söderman, O. *J. Magn. Reson. A.* **1993**, *104*, 17–25.
- (22) (a) Strang, G. *Linear Algebra and its Applications*; Harcourt, **1988**. (b) Stewart, G.W. *Introduction to Matrix Computations*; Academic Press: New York, 1973.
- (23) Basser, P.J. *Magn. Reson. Med.* **2002**, *47*, 392–397.
- (24) (a) Assaf, Y.; Mayk, A.; Cohen, Y. *Magn. Reson. Med.* **2000**, *44*, 713–722. (b) Assaf, Y.; Ben-Bashat, D.; Chapman, J.; Peled, S.; Biton, I.E.; Kafri, M.; Segev, Y.; Hendler, T.; Korczyn, A.D.; Graif, M.; Cohen, Y. *Magn. Reson. Med.* **2002**, *47*, 392–397. (c) Assaf, Y.; Mayzel-Oreg, O.; Gigi, A.; Ben-Bashat, D.; Mordohovitch, M.; Verchovsky, R.; Reider-Groswasser, II.; Hendler, T.; Graif, M.; Cohen, Y.; Korczyn, A.D. *J. Neurol. Sci.* **2002**, *203–204*, 235–239. (d) Wedeen, V.J.; Reese, T.G.; Tuch, D.S.; Weigel, M.R.; Dou, J-G.; Weisskoff, R.M.; Chessler, D. In *Proceedings 8th Annual Meeting of ISMRM*; 2000, p 82.
- (25) Pach, K.; Frey, T. *Vector and Tensor Analysis*; Terra: Budapest, 1964.
- (26) Basser, P.J.; Pjevic, S.; Pierpaoli, C.; Duda, J.; Aldroubi, A. *Magn. Reson. Med.* **2000**, *44*, 625–632.